Photophysical Properties of a Three-Dimensional Zinc(II) Porphyrin Box

In-Wook Hwang, Hyun Sun Cho, Dae Hong Jeong,[†] and Dongho Kim*

Center for Ultrafast Optical Characteristics Control and Department of Chemistry, Yonsei University, Seoul 120-749, Korea

Akihiko Tsuda, Takashi Nakamura, and Atsuhiro Osuka*

Department of Chemistry, Graduate School of Science, Kyoto University, Kyoto 606-8502, Japan

Photophysical properties of a three-dimensional zinc(II) porphyrin box ((PyZ2)$_4$) and its constituent unit (orthogonally linked porphyrin dimers such as PyZ2 and Z2) have been comparatively investigated by absorption, fluorescence, picosecond time-resolved fluorescence/fluorescence anisotropy, resonance Raman, and femtosecond transient absorption measurements. The negligible temperature dependence on the fluorescence and fluorescence excitation spectra of PyZ2 in CH$_2$Cl$_2$ indicates that the porphyrin box is not easily disorganized in the temperature range of ∼10−40 °C. The enhancement of a short-lived (∼1 ns) fluorescence decay component, as well as the shifts of the ν_2 and ν_4 Raman bands, indicates that the porphyrin ring planarity is somewhat perturbed, because of the five-coordination of the zinc(II) porphyrin moiety in the porphyrin box. The relatively slow rotational diffusion time of ∼4.7 ns and $r_\infty = 0$ in the time-resolved fluorescence anisotropy decay measurement illustrates that the porphyrin box rotates more slowly than the porphyrin dimers (PyZ2 and Z2), because of its large molecular volume. In addition, the fast anisotropy rise time of 12 ± 3 ps in the femtosecond transient absorption anisotropy decay measurement reflects an excitation energy-transfer process in the porphyrin box. The red-shifted high-energy Soret band and the blue-shifted low-energy Soret band of the porphyrin box are indicative of excitonic dipole−dipole interactions between four parallel transition dipole moments along the *x*- or *y*-axis and between eight parallel transition dipole moments along the *z*-axis of the box. This process is regarded as a dipole redistribution process within the three-dimensional zinc(II) porphyrin box.

Introduction

Various porphyrin arrays have been intensively investigated recently, because of their unique electrical and optical properties as promising candidates for light harvesting,[1] photosynthetic reaction,[2] photodynamic therapy,[3] and electronic communication[4] systems. Currently, much effort has been directed toward the synthesis and characterization of porphyrin oligomers that contain three or more covalently linked porphyrin molecules. Recently, we have performed various spectroscopic studies on one- or two-dimensional orthogonal[5,6] and fused[7] porphyrin arrays in which the porphyrins are directly linked by covalent bonds without any linkers. In the meantime, supramolecular chemistry, using a strategy of noncovalent self-assembly of molecular units, has also been established as a highly promising method, from a viewpoint of constructing two- or three-dimensional porphyrin architectures that are suitable for efficient light harvesting and energy-transport systems.[8−10] This approach often uses electrostatic interactions between positive central metal ions and negative peripheral substituents of metalloporphyrins.[8−11] Thus, in this study, we have prepared a three-dimensional porphyrin box, using a self-assembly of pyridyl-substituted orthogonally linked zinc(II) porphyrin dimer (PyZ2),

and investigated its photophysical properties in comparison with its constituent units (Z2 and PyZ2).

As shown in Scheme 1, a three-dimensional zinc(II) porphyrin box ((PyZ2)$_4$) has been formed by a self-assembly of orthogonally linked porphyrin dimer (PyZ2) that has two pyridyl groups at two meso-positions.[12] PyZ2 molecules self-assemble into the three-dimensional zinc(II) porphyrin box, because of intermolecular coordination between the Zn^{2+} central metal ion of PyZ2 and the peripheral pyridyl group of neighboring PyZ2. The intermolecular coordination implies the coordination between PyZ2 molecules, but not the covalent bonding between zinc(II) porphyrin monomers within PyZ2. The structural characterization of the zinc(II) porphyrin box was previously confirmed using procedures such as ^{1}H NMR spectroscopy, gel-permeable chromatography (GPC), and cold spray ionization−mass spectroscopy (CSI−MS) in which the porphyrin box revealed a large association constant—at least 10^{25} M^{-3} in nonligating CHCl$_3$ solvent—which assured a stable organization up to 1.6×10^{-8} M.[12] The stable porphyrin box (PyZ2)$_4$ was inferred from gel-permeable chromatography−high-pressure liquid chromatography (GPC−HPLC) with CHCl$_3$ as an eluent.[12] (PyZ2)$_4$ exhibited a sharp elution band, with a distinctly shorter retention time (13.9 min) than that of Z2 (16.3 min), which suggests the preservation of the discrete (PyZ2)$_4$ aggregate. In addition, the CSI−MS analysis detected the parent ion of (PyZ2)$_4$ at 6258, which is exactly the position expected for (PyZ2)$_4$ (the calculated M_r value for C$_{376}$H$_{400}$N$_{40}$O$_{16}$Zn$_8$ is 6258).[12] Nevertheless,

SCHEME 1

Ar^2 =

Z2

PyZ2 in pyridine

(PyZ2)$_4$ in CH$_2$Cl$_2$
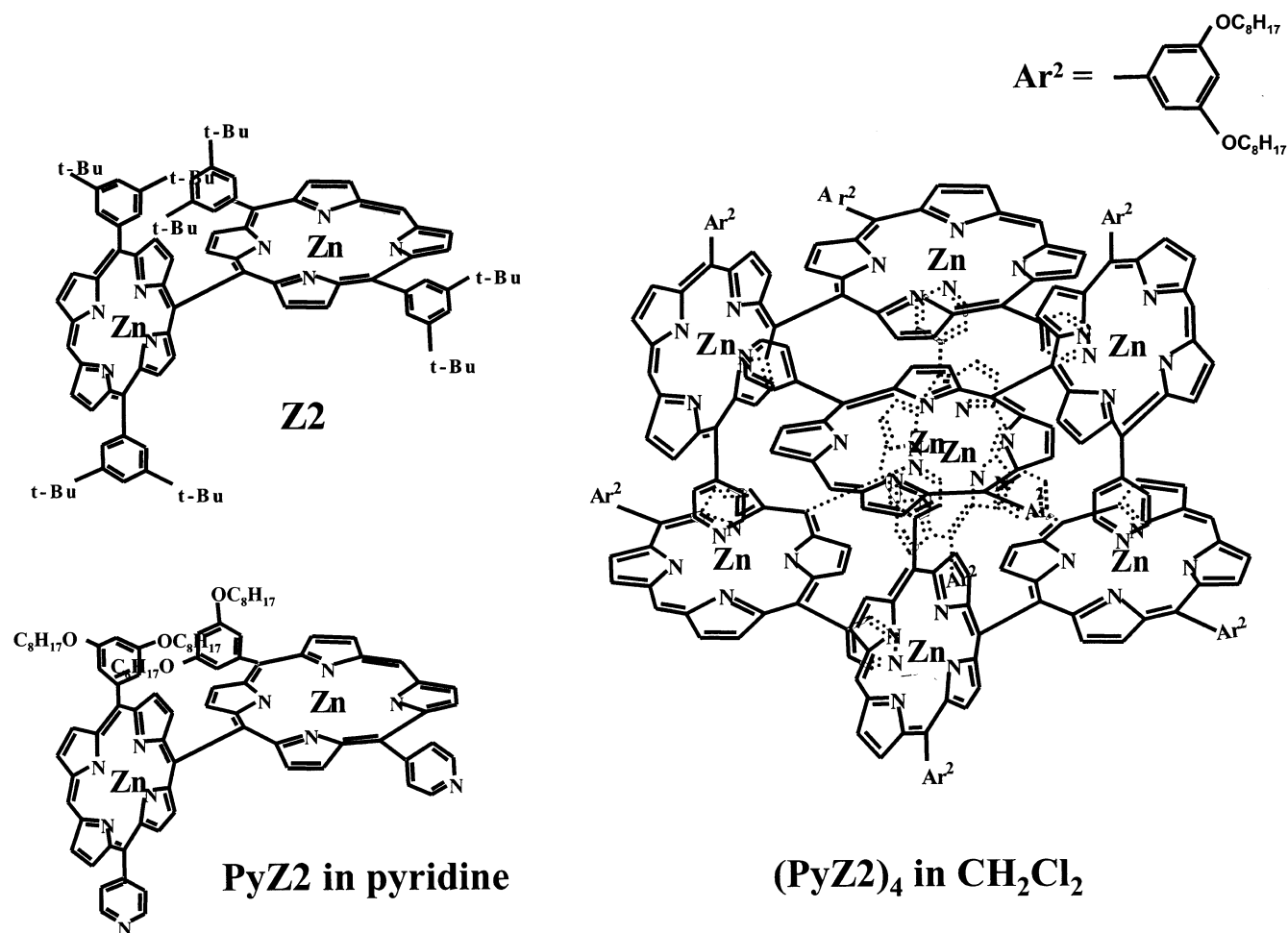
because the intermolecular coordination between PyZ2 molecules competes with the solvent coordination as an axial ligand of the zinc(II) porphyrin monomer moiety in PyZ2, the box formation of PyZ2 is significantly dependent on the solvent ligating ability. More specifically, PyZ2 molecules self-assemble into the porphyrin box in CH$_2$Cl$_2$, whereas they remain as porphyrin dimers in pyridine (see Scheme 1).[12] The CH$_2$Cl$_2$ solvent does not have the capability to coordinate with zinc(II) porphyrin as an axial ligand, because of its absence of nonpaired electrons, while pyridine solvent can coordinate with zinc(II) porphyrin, because of its nonpaired electrons. As a consequence, the box formation of PyZ2 only occurs in CH$_2$Cl$_2$, where the intermolecular coordination predominantly occurs over the solvent coordination. In contrast to PyZ2, Z2 does not experience intermolecular coordination in any solvents, because of its absence of appropriate peripheral substituents (see Scheme 1). Thus, we use Z2 as a reference molecule of PyZ2 in investigating the intermolecular coordination dynamics of the orthogonally linked porphyrin dimer in various solvent conditions.

In our study, the competition between the solvent and intermolecular coordinations of the orthogonally linked porphyrin dimers (Z2 and PyZ2) has been investigated in three different solvents: CH$_2$Cl$_2$, tetrahydrofuran (THF), and pyridine. The photophysical properties of the solvent and intermolecular coordinated porphyrin dimers have been comparatively investigated by absorption, fluorescence, picosecond time-resolved fluorescence/fluorescence anisotropy, and resonance Raman (RR) spectroscopy, as well as femtosecond transient absorption spectroscopy. The temperature-dependent fluorescence and

fluorescence excitation spectra were also recorded to explore the unfolding or the stability of the porphyrin box. The absorption and fluorescence spectra have provided information on the ligations of the porphyrin assemblies in various environments. Time-resolved fluorescence decay measurements have been conducted to monitor the excited-state dynamics of the porphyrin assemblies. Fluorescence anisotropy decay measurements were used to reveal the rotational diffusion motions of the molecules.[13,14] Femtosecond transient absorption anisotropy measurements were adopted to examine the fast energy-transfer process of the porphyrin box. RR spectroscopy was used to investigate the specific vibrational modes of the solvent and intermolecular coordinated porphyrin assemblies.

Experimental Section

Sample Preparation and Steady-State Spectroscopic Measurements. The synthetic procedures of Z2[15] and PyZ2[12] were previously reported. Z2 and PyZ2 were prepared in approximately micromolar concentrations in CH$_2$Cl$_2$, THF, and pyridine solvents. All the solvents (∼99.9% purity) were purchased from Merck Chemical Co. (HPLC grade). Absorption spectra were obtained with a Shimadzu model 1601 UV spectrometer, and steady-state fluorescence and excitation spectra were measured by a Hitachi model F-4500 fluorescence spectrophotometer. A temperature-controlling circulator (JEIO TECH model VTRC-640) coupled to the fluorescence cell was used for the temperature-dependent measurements. Applied temperature ranges were ∼10−60 °C for the THF solution and ∼10−40 °C for the CH$_2$Cl$_2$ solution, because of the boiling

Photophysical Properties of 3D Zinc(II) Porphyrin

J. Phys. Chem. B, Vol. 107, No. 37, 2003 **9979**

points of the solvents (i.e., 66 °C of THF and 40 °C of CH$_2$Cl$_2$). Steady-state fluorescence and excitation measurements during heating were maintained for ∼20 min before each measurement, to equilibrate the sample temperatures.

Time-Resolved Fluorescence Decay Measurements. A picosecond time-correlated single photon counting (TCSPC) system was used for time-resolved fluorescence and fluorescence anisotropy decay measurements.[16] The system consisted of a self-mode-locked and cavity-dumped femtosecond Ti:sappahire laser pumped by a continuous wave (cw) Nd:YAG laser (Coherent, Verdi). The full width at half-maximum of the instrument response function obtained by a dilute solution of coffee cream was typically 50 ps in our TCSPC system. The fluorescence decays were measured with magic-angle emission polarization, and the number of fluorescence photons per unit time, detected by a photomultiplier tube, was always maintained to be <1% of the repetition rate of the excitation pulses, to prevent pile-up distortions in the decay profiles. Time-resolved fluorescence anisotropy decays were obtained by changing the detection polarization on the fluorescence path parallel or perpendicular to the polarization of the excitation light. The anisotropy decays then were calculated as follows:

$$r(t) = \frac{I_{VV}(t) - GI_{VH}(t)}{I_{VV}(t) + 2GI_{VH}(t)}$$

where $I_{VV}(t)$ (or $I_{VH}(t)$) is the fluorescence decay when the excitation light is vertically polarized and only the vertically (or horizontally) polarized portion of fluorescence is detected, denoting that the first and second subscripts represent excitation and detection polarization, respectively. The factor G is defined by $I_{VV}(t)/I_{VH}(t)$, which is equal to the ratio of the sensitivities of the detection system for vertically and horizontally polarized light. The G factor of our detection system was 1.08. The fittings for both isotropic and anisotropic decays were performed by a least-squares deconvolution fitting process.[17] The vertical and horizontal components of fluorescence emission were simultaneously fitted to extract the anisotropy decay functions, using the LIFETIME program with an iterative nonlinear least-squares deconvolution procedure that was developed at the University of Pennsylvania.[18]

Ground-State Raman Spectrum Measurements. Ground-state RR spectra were obtained by photoexcitation, using the 457.9 nm line of a cw argon-ion laser (Coherent model INNOVA 90). This line corresponds to the low-energy exciton split Soret bands of the porphyrin dimers, as well as the porphyrin box. Raman scatterings were collected in a 90° scattering geometry and detected by a single-pass spectrometer (Acton Research model 500i) with a liquid-nitrogen-cooled charge-coupled device (PI model LN/CCD-1152E).

Transient Absorption Anisotropy Decay Measurements. The dual-beam femtosecond time-resolved transient absorption spectrometer consisted of a self-mode-locked femtosecond Ti: sapphire oscillator (Coherent, MIRA), a Ti:sapphire regenerative amplifier (Clark MXR model CPA-1000) that was pumped by a Q-switched Nd:YAG laser (Clark MXR model ORC-1000), a pulse stretcher/compressor, an optical parametric amplifier (Light Conversion, TOPAS) system, and an optical detection system. A femtosecond Ti:sapphire oscillator pumped by a cw Nd:YVO$_4$ laser (Coherent, Verdi) produces a train of ∼80-fs mode-locked pulses with an averaged power of 650 mW at 800 nm. The amplified output beam regenerated by chirped pulse amplification had a pulse width of ca. 150 fs and a power of ca. 1 W at a repetition rate of 1 kHz, which was divided into

two parts by a 1:1 beam splitter. One part was frequency-doubled for the pump beam by a β-BBO crystal. The pump beam was focused to a spot diameter of 1 mm, and the laser fluence was adjusted to avoid damaging the sample, using a variable neutral-density filter. The other part was focused onto a flowing water cell to generate a white-light continuum, which was again split into two parts. One part of the white-light continuum was overlapped with the pump beam at the sample to probe the transient, while the other part of the white-light continuum beam was passed through the sample without overlapping the pump beam. The time delay between pump and probe beams was controlled by making the pump beam travel along a variable optical delay line. The white-light continuum beams after the sample were sent through an appropriate interference filter and then were detected by two photodiodes. The outputs from the two photodiodes at the selected wavelength were processed by a combination of a boxcar averager and a lock-in amplifier, to calculate the absorption difference spectrum at the desired time delay between pump and probe pulses. For the transient absorption anisotropy decay ($r(t)$) measurements, the probe white-light continuum pulse was set to have vertical polarization using a sheet polarizer. The excitation pulse then was changed to have parallel or perpendicular polarization by rotating a half wave plate centered at 400 nm, with respect to the polarization of the probe pulse. Finally, the transient absorption anisotropy decay can be obtained by the following equation:[6]

$$r(t) = \frac{\Delta A_{VV}(t) - \Delta A_{HV}(t)}{\Delta A_{VV}(t) + 2\Delta A_{HV}(t)}$$

where the variable represents amplitude.

Results and Discussion

Solvent and Intermolecular Coordination of Z2 and PyZ2 in Various Solvents. Figures 1 and 2 respectively show the absorption and fluorescence spectra of Z2 and PyZ2 in various solvents. The solvent and intermolecular coordinations for the respective panels in each figure are as follows: (a) Z2 in CH$_2$Cl$_2$ (nonsolvent coordination), (b) Z2 in THF (weak solvent coordination), (c) Z2 in pyridine (strong solvent coordination), (d) PyZ2 in pyridine (strong solvent coordination), (e) PyZ2 in THF (loose intermolecular coordination), and (f) PyZ2 in CH$_2$Cl$_2$ (tight intermolecular coordination). Table 1 reveals the band maxima of the absorption and fluorescence spectra. CH$_2$Cl$_2$ solvent cannot coordinate with Z2, but THF and pyridine solvents can coordinate weakly and strongly with Z2 as axial ligands, respectively, because of their nonpaired electrons and ligating abilities. PyZ2 experiences strong solvent coordination in pyridine, because the pyridine solvent is predominant over the peripheral pyridyl group of PyZ2 in coordinating with the central Zn^{2+} ion of the neighboring PyZ2, which is due to its reduced steric hindrance and larger abundance. On the other hand, PyZ2 results in the box formation in THF and CH$_2$Cl$_2$, because these solvents are not stronger than the peripheral pyridyl group of PyZ2 in coordinating with the central Zn^{2+} ion of the neighboring PyZ2.[12] The intermolecular coordination is also tighter in CH$_2$Cl$_2$ than in THF, because the polar (electrostatic) intermolecular interaction becomes strong in a nonpolar CH$_2$Cl$_2$ solvent.[19]

The absorption spectra of Z2 and PyZ2 are characteristic of the orthogonally linked porphyrin dimers: exciton split Soret transitions (S$_0$→S$_2$) in the short-wavelength region of ∼400−500 nm.[5,6] The absorption spectra reveal coordination strength

TABLE 1: Band Maxima of Absorption and Fluorescence Spectra of Z2 and PyZ2 in Various Solvents[a]

solvent	Absorption[b] (nm)				Fluorescence (nm)	
	Soret (high)	Soret (low)	$Q(1,0)$	$Q(0,0)$	$Q(0,0)$	$Q(0,1)$
			Sample Z2			
CH$_2$Cl$_2$	414.3 (24 135)	447.5 (22 341)	553	591	619	651
THF	417.2 (23 970)	451.7 (22 138)	560	600	625	660
pyridine	425.4 (23 516)	459.7 (21 755)	569	610	634	671
			Sample PyZ2			
pyridine	424.9 (23 535)	460.3 (21 724)	567	607	633	672
THF	419.6 (23 835)	449.8 (22 231)	561	603	613	665
CH$_2$Cl$_2$	426.7 (23 457)	447.9 (22 328)	565	606	616	669

[a] The band position was determined by Gaussian band fitting process. [b] Values shown in parentheses are absorption positions given in units of cm^{-1}.
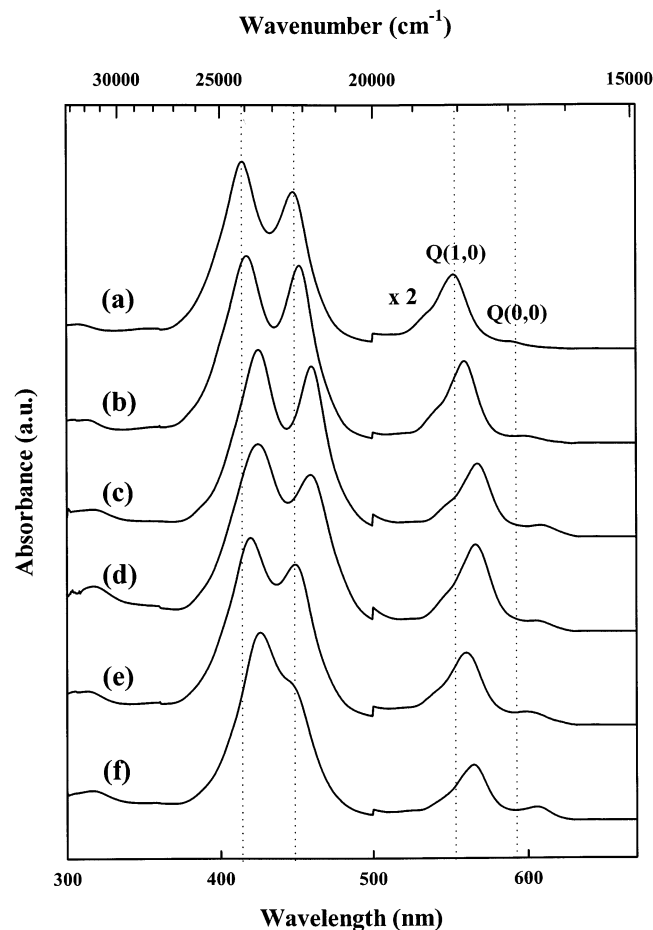

Figure 1. Absorption spectra of (a) Z2 in CH$_2$Cl$_2$, (b) Z2 in THF, (c) Z2 in pyridine, (d) PyZ2 in pyridine, (e) PyZ2 in THF, and (f) PyZ2 in CH$_2$Cl$_2$. Intensities of the Q bands were multiplied by a factor of 2.

dependence such that the high-energy Soret and Q bands are red-shifted, the Q(0,0) band is enhanced as the solvent coordination strength increases (Figure 1a–d), and the box formation occurs (Figure 1e,f). These spectral features are in good agreement with the typical spectroscopic observations on the axial-ligand coordination of the metalloporphyrin monomers. Generally, Soret and Q bands are red-shifted and the Q(0,0) band is enhanced as the axial coordination occurs in the metalloporphyrin monomers.[9,20] The largely red-shifted high-energy Soret and Q bands, as well as the strongly enhanced Q(0,0) band in Figure 1f, in comparison with those of Figure 1a, strongly suggest intermolecular coordination i.e., box formation between PyZ2 molecules in the nonligating CH$_2$Cl$_2$ solvent. However, the low-energy Soret band in Figure 1f exhibits somewhat different characteristics from the results of

ligated metalloporphyrin monomers. The low-energy Soret band in Figure 1 is red-shifted from Figure 1a to Figure 1c and d as the solvent coordination strength increases, whereas it is unexpectedly blue-shifted in Figure 1e and f as the box formation is enhanced. Thus, the blue-shifted low-energy Soret band is regarded as a unique feature of the zinc(II) porphyrin box. This blue shift is explained by excitonic dipole−dipole couplings within the three-dimensional zinc(II) porphyrin box (vide infra).

The fluorescence spectra of Z2 and PyZ2 are displayed in Figure 2, where the excitation wavelength dependence is negligible. The fluorescence spectra are gradually red-shifted as the solvent coordination strength increases from Figure 2a to Figure 2c and d, whereas they are blue-shifted and remain at similar positions in Figure 2e and f. It is also observed that the relative intensity of the Q(0,0) fluorescence sub-band at short wavelengths becomes strong in going from Figure 2a to Figure 2c and d, as well as from Figure 2e to Figure 2f. Both red-shifted fluorescence spectra and the Q(0,0) sub-band fluorescence enhancement are also characteristics of ligated metalloporphyrins.[9,20] However, the blue-shifted fluorescence spectra in Figure 2e and f are not consistent with the reported characteristics of ligated metalloporphyin monomers. These blue-shifted fluorescence spectra are likely to originate from the intrinsic feature of the self-assembly of the orthogonally linked porphyrin dimer (PyZ2). This may be rationalized in terms of the enhanced rigidification in the (PyZ2)$_4$ assembly, where the two porphyrins in a meso−meso linked diporphyrin are forced to take a rigorously perpendicular orientation, thus minimizing the electronic interaction between the porphyrin monomer units. Although the blue-shifted absorption spectrum of the porphyrin box is due to excitonic interaction between the porphyrin units (vide infra), the blue-shifted fluorescence spectrum cannot have an excitonic origin in view of weak transition dipole moment of the lowest excited singlet S$_1$ state of the porphyrin. The constrained molecular flexibility generally results in the blue-shifted fluorescence, as compared to that of a free molecule, because of the reduced Stokes shift of the fluorescence center.[21]

To investigate thermal perturbation effect on the self-assembly of PyZ2, the temperature-dependent fluorescence and its excitation spectra of PyZ2 are measured in THF (Figure 3) and CH$_2$Cl$_2$ (Figure 4). As the temperature increases in THF, the fluorescence excitation spectra reveal larger Soret band splitting, as well as a reduced Q(0,0) excitation band (Figure 3a). In addition, the fluorescence intensity continuously decreases and an isoemissive point appears in the normalized fluorescence spectra (Figure 3b). The fluorescence intensity decreases as the temperature increases, because of the enhanced thermal deactivation process; therefore, the normalized fluorescence spectra are used to monitor the change in the molecular coordination. With consideration of the absorption and fluorescence spectral
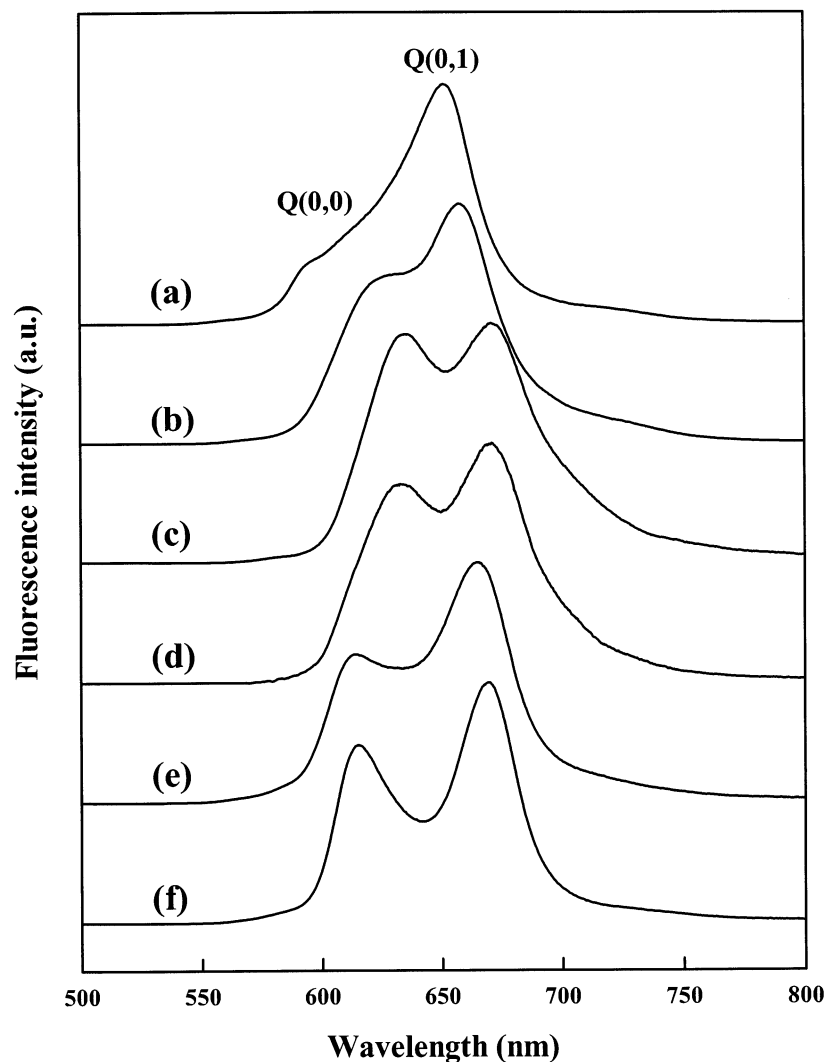
Figure 2. Steady-state fluorescence spectra of (a) Z2 in CH₂Cl₂, (b) Z2 in THF, (c) Z2 in pyridine, (d) PyZ2 in pyridine, (e) PyZ2 in THF, and (f) PyZ2 in CH₂Cl₂. Excitation wavelengths were 416 nm for Z2 and 430 nm for PyZ2.

characteristics, depending on the solvent and intermolecular coordinations of Z2 and PyZ2 (Figures 1 and 2), we conclude that the box formation of PyZ2 is disturbed toward solvent ligation or nonligation in THF as the temperature increases (Figure 3). The isoemissive point clearly indicates the ground-state coordination transition of PyZ2 in THF. In contrast, the fluorescence excitation and fluorescence spectra of PyZ2 in CH₂Cl₂ exhibit negligible temperature dependence (see Figure 4). This suggests that the tight intermolecular coordination of PyZ2, i.e., the box formation, is not easily disturbed in the applied temperature range of ∼10−40 °C in CH₂Cl₂.

Fluorescence Lifetimes and Rotational Diffusion Motions of Porphyrin Dimer and Porphyrin Box. The time-resolved fluorescence decays of the porphyrin molecules are displayed in Figure 5, and their fitted parameters are tabulated in Table 2. As listed in Table 2, the orthogonally linked zinc(II) porphyrin dimers (Z2, PyZ2) typically exhibit faster fluorescence decays (τ_{avg}) than the zinc(II) porphyrin monomer (2.64 ns). According to the previous reports on the orthogonally linked zinc(II) porphyrin arrays, the fluorescence lifetime gradually decreases to exhibit an asymptotic feature as the number of porphyrin units increases in the arrays, which is due to the increased conformational heterogeneity in longer arrays.[5] As shown in Figure 5, the fluorescence decay of Z2 reveals a slight dependence on the solvent used. The exponential fittings for all the decay curves were performed with two decay components

and gave desirable χ^2 values (∼1.0−1.3), as listed in Table 2. According to the reported fluorescence lifetimes on the orthogonally linked porphyrin arrays,[5,6] and the self-assembled zinc(II) porphyrin tetramer,[22] as well as various nonplanar free-base porphyrin monomers,[23] two fluorescence decay components of the porphyrin units are known to originate from the conformational heterogeneity of porphyrins such as planar and nonplanar conformers. In addition, the self-assembled zinc(II) porphyrin tetramer showed comparable values of τ_1 and τ_2 in Table 2: fluorescence lifetimes of ∼1.5 and ∼2 ns in the ligated and nonligated conditions, respectively.[22] Therefore, the two fluorescence decay components can be correlated with the conformational heterogeneities of the porphyrin units. A systematic variation in the fluorescence decay components is observed, depending on the solvent and intermolecular coordinations of Z2 and PyZ2. Especially, the relative amplitude of the fast decay component (τ_1) gradually increases as the coordination strength increases (Table 2). Consequently, τ_1 originates from a nonplanar porphyrin conformer, the formation of which is enhanced by solvent or intermolecular coordination. On the other hand, the slow decay component (τ_2) originates from planar porphyrin conformer. The relatively fast fluorescence decay ($\tau_{avg} \approx 1.5$ ns) of the porphyrin box results from the enhanced nonplanarity of the porphyrin macrocycle by strong intermolecular coordination in the porphyrin box, which leads
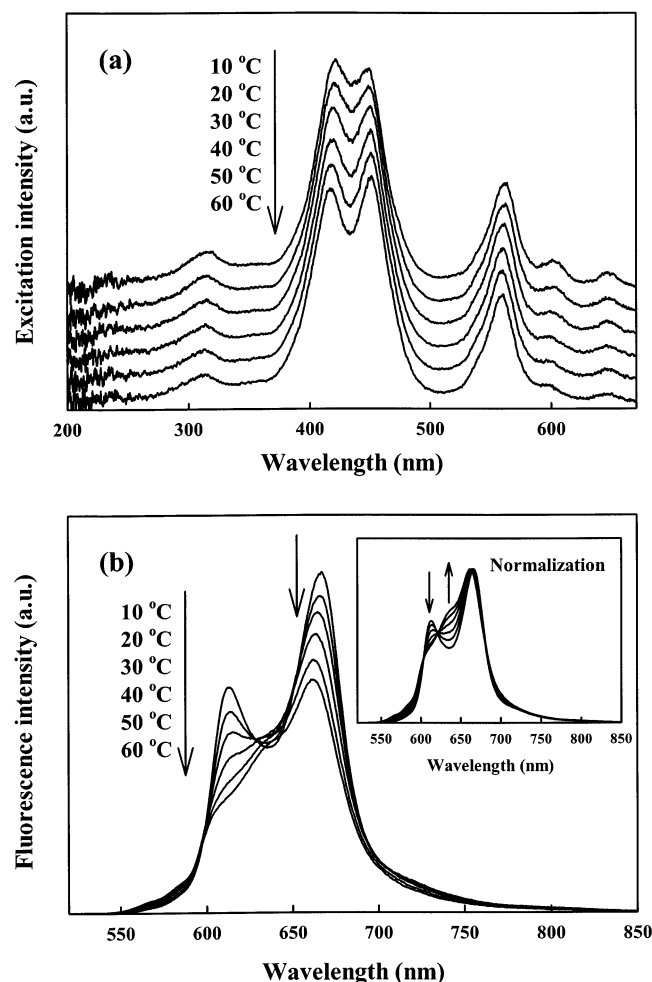
Figure 3. Temperature-dependent (a) fluorescence excitation and (b) fluorescence spectra of PyZ2 in THF. The applied temperature range was ∼10−60 °C, and the inset shows the normalized fluorescence spectra.
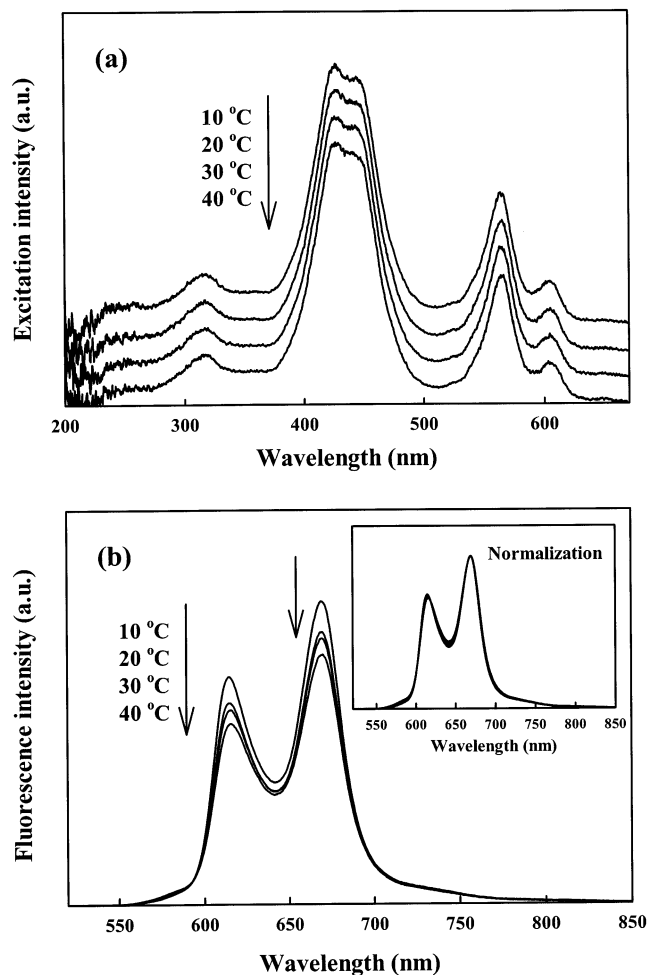

Figure 4. Temperature-dependent (a) fluorescence excitation and (b) fluorescence spectra of PyZ2 in CH₂Cl₂. The applied temperature range was ∼10−40 °C, and the inset shows the normalized fluorescence spectra.

TABLE 2: Fitted Fluorescence Lifetimes of Z2 and PyZ2 in Various Solvents[a]

solvent	detection wavelength of emission, λ_{em}[b] (nm)	Fitted Fluorescence Lifetimes (ns)		
		τ_1	τ_2	τ_{avg}
		Sample Z2		
CH₂Cl₂	600	0.73 (9%)	1.85 (91%)	1.63
	650	0.73 (10%)	1.86 (90%)	1.60
THF	625	0.99 (11%)	2.15 (89%)	1.91
	650	0.98 (11%)	2.15 (89%)	1.90
Pyridine	620	0.87 (21%)	2.07 (79%)	1.61
	670	0.90 (22%)	2.07 (78%)	1.61
		Sample PyZ2		
Pyridine	620	1.08 (22%)	1.99 (78%)	1.67
	670	1.04 (23%)	1.93 (77%)	1.62
THF	613	1.18 (31%)	2.19 (69%)	1.73
	667	1.16 (35%)	2.26 (65%)	1.70
CH₂Cl₂	615	1.00 (32%)	1.97 (68%)	1.50
	670	1.00 (33%)	2.02 (67%)	1.51

[a] Using the relation $I(t) = A_1 \exp(-t/\tau_1) + A_2 \exp(-t/\tau_2)$, where $I(t)$ is the time-dependent fluorescence intensity, A the amplitude (noted in parentheses as the normalized percentage of $\tau_1 = [A_1\tau_1/(A_1\tau_1 + A_2\tau_2)] \times 100$), τ the fitted fluorescence lifetime, λ_{em} the detection wavelength of emission, and τ_{avg} the averaged fluorescence lifetime ($\tau_{avg} = (A_1\tau_1 + A_2\tau_2)/(A_1 + A_2)$). [b] The excitation wavelength, 403 nm, was applied to all samples. The χ^2 values of the fittings were maintained as ∼1.0−1.3.

to mean plane deviation by pulling the central Zn^{2+} ion out of the plane by ∼0.05 Å.[12]

The fluorescence anisotropy decay profiles of the porphyrins are presented in Figure 6, and their fitted parameters are tabulated in Table 3. All the fluorescence anisotropy decays have negative amplitudes and converge to zero at $t = \infty$. The negative anisotropies suggest incoherent energy-hopping processes between the porphyrin monomers in the orthogonally linked porphyrin dimers. These processes proceed on the time scale of ∼200 fs, according to our previous report on the orthogonally linked porphyrin arrays.[6] The zero convergence of the anisotropy decay indicates a nonbox polymer formation of the zinc(II) porphyrin box, which is consistent with the previous characterization of (PyZ2)₄ using ¹H NMR spectroscopy.[12] As shown in Figure 6 and Table 3, the rotational diffusion times are systematically dependent on the solvent and intermolecular coordinations of the porphyrins. Z2 shows relatively fast rotational diffusion times of ∼400 ps in CH₂Cl₂ and 500 ps in THF, whereas the rotational diffusion motion slows, with a time constant of ∼1.2 ns in pyridine, which is due to strong solvent coordination. In PyZ2, a rotational diffusion time of ∼1.9 ns is observed in pyridine, which is somewhat different from the time constant of 1.2 ns for Z2 in pyridine. This variation seems to originate from different molecular volumes of peripheral substituents of the porphyrin dimers, i.e., 3,5-dioctyloxyphenyls of PyZ2 and 3,5-di-*tert*-butylphenyls of Z2, as presented in Scheme 1. The box formation of PyZ2 in CH₂Cl₂ results in a much slower rotational decay time of ∼4.7 ns, because of its larger molecular volume.

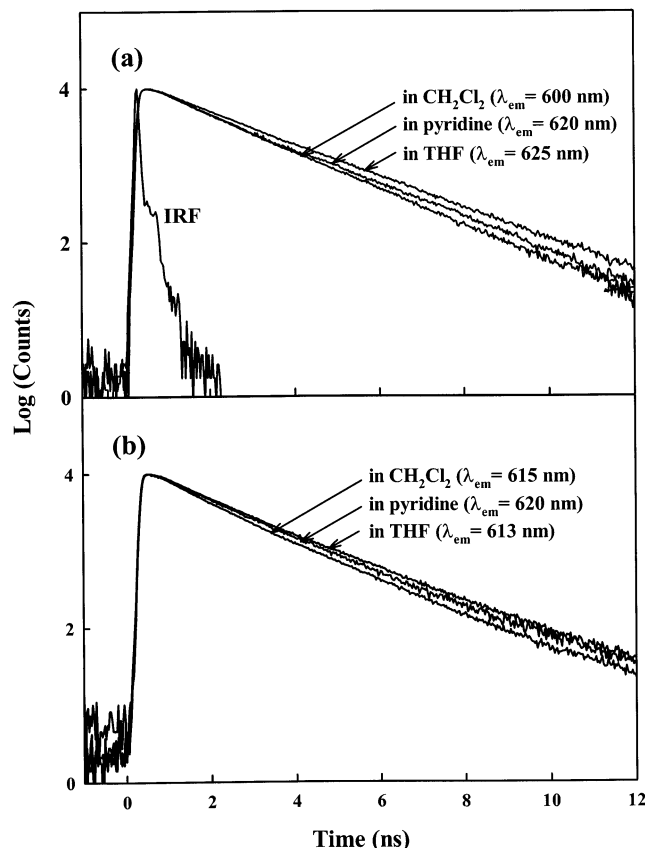**Figure 5.** Time-resolved fluorescence decay profiles of (a) Z2 and (b) PyZ2 in CH$_2$Cl$_2$, pyridine, and THF solvents. IRF represents the instrument response function of the TCSPC system.

In contrast, PyZ2 in THF reveals a rotational diffusion time of ~1.4 ns, which may be due to the result of averaging the rotational diffusion rates of the PyZ2 dimer and the (PyZ2)$_4$ box. The double exponential fitting for the anisotropy decay in Figure 6e is not satisfactory, because of its large noise level. It is also observed in Table 3 that the average angles (δ) between absorption and emission dipoles are consistent, regardless of the solvent and intermolecular coordinations. This observation means that the orthogonal geometry of PyZ2 is unlikely to be changed by the solvent or intermolecular coordination, even in the self-assembled porphyrin box. Finally, the porphyrin box shows a relatively small r_0 value (approximately −0.007), with respect to the porphyrin dimers (r_0 = −0.018 to −0.027). This result is indicative of different depolarization channels of the porphyrin box, in comparison to the porphyrin dimers (vide infra).

Resonance Raman Spectroscopic Measurements. To have detailed information on the molecular structures of the porphyrins, the resonance Raman (RR) spectra of Z2 and PyZ2 in various solvents are measured and shown in Figure 7 (Z2 in THF is shown in panel a, PyZ2 in pyridine in panel b, PyZ2 in THF in panel c, and PyZ2 in CH$_2$Cl$_2$ in panel d). The Raman band assignments of PyZ2 in pyridine, THF, and CH$_2$Cl$_2$ are tabulated in Table 4, in which the assignments are based on the previous Raman modes of Z2 in THF.[24] In Figure 7, PyZ2 and Z2 reveal similar RR spectra, except for a 12 cm^{-1} downshift of the Φ_{10} band in PyZ2, which is due to a pyridyl substitution effect. Note that the low-frequency Raman bands, such as ν_{35}, Φ_{10}, ν_8, ν_{33}, ν_{49}, and Φ_9 modes, become significantly weak in Figure 7c and d, with respect to Figure 7a and b. These low-frequency Raman bands are mainly associated with C$_m$−
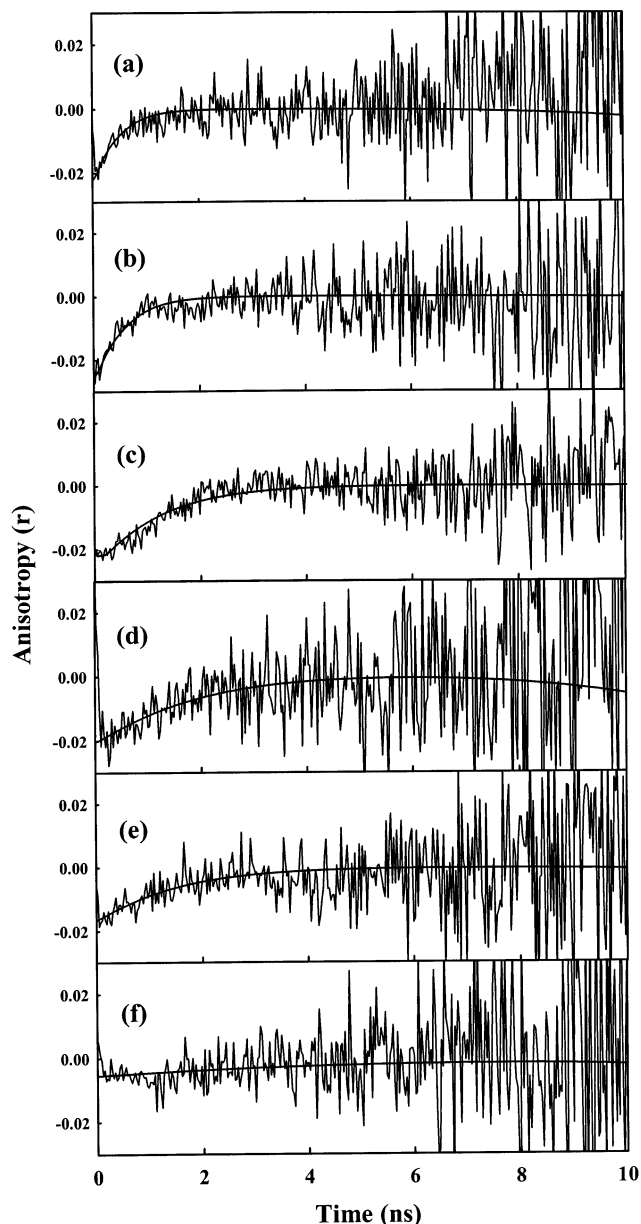

Figure 6. Time-resolved fluorescence anisotropy decay profiles and their fitted lines of (a) Z2 in CH$_2$Cl$_2$, (b) Z2 in THF, (c) Z2 in pyridine, (d) PyZ2 in pyridine, (e) PyZ2 in THF, and (f) PyZ2 in CH$_2$Cl$_2$. The fluorescence anisotropy decays were obtained with high-energy Soret band excitations (λ_{ex} = 403 nm) and Q(0,0) fluorescence detections.

C$_\alpha$ and nitrogen−metal (N−M) stretching/bending modes of the porphyrin units, according to the normal-mode analyses of nickel porphyrin monomers.[25] Accordingly, the weak low-frequency Raman bands in Figure 7c and d illustrate that the intermolecular coordination of PyZ2 restricts C$_m$−C$_\alpha$ and N−M stretching/bending motions of the porphyrin units in the porphyrin box. The very weak ν_{35} and ν_{33} Raman bands in Figure 7d suggest that the rigid box formation of PyZ2 constrains pyrrole rotation and translation motions appreciably in the porphyrin units.

In contrast to the low-frequency Raman bands, high-frequency Raman bands do not show significant spectral variations. However, it is recognizable in Table 4 that the structure-sensitive Raman bands, such as the ν_4 and ν_2 modes[26,27] of the porphyrin moiety, are slightly downshifted through the box formation. These shifts indicate that the planarity of the porphyrin unit is more perturbed by the box formation of PyZ2 than in the

TABLE 3. Emission Anisotropy Decay Parameters of Z2 and PyZ2 in Various Solvents[a]

solvent	detection wavelength of emission, λ_{em}[b] (nm)	r_0	fitted rotational decay time, Φ (ns)	average angle between absorption and emission dipoles, δ (deg)
		Sample Z2		
CH$_2$Cl$_2$	600	-0.024 ± 0.002	0.41 ± 0.04	57.3
	650	-0.023 ± 0.003	0.41 ± 0.05	57.1
THF	625	-0.027 ± 0.002	0.50 ± 0.06	57.5
	650	-0.018 ± 0.004	0.50 ± 0.09	56.6
pyridine	620	-0.021 ± 0.002	1.16 ± 0.15	56.9
	670	-0.020 ± 0.003	1.18 ± 0.12	56.8
		Sample PyZ2		
pyridine	620	-0.021 ± 0.003	1.88 ± 0.23	56.9
	670	-0.027 ± 0.003	1.86 ± 0.22	57.5
THF	613	-0.017 ± 0.002	1.45 ± 0.21	56.5
	667	-0.013 ± 0.002	1.42 ± 0.24	56.1
CH$_2$Cl$_2$	615	-0.006 ± 0.002	4.90 ± 1.10	55.3
	670	-0.008 ± 0.002	4.50 ± 0.80	55.6

[a] Using the relation $r(t) = r_0 \exp(-t/\Phi)$, where $r(t)$ is the time-dependent fluorescence anisotropy ($r(t) = (I_{||}(t) - GI_{\perp}(t))/(I_{||}(t) + 2GI_{\perp}(t))$), Φ the fitted rotational decay time, λ_{em} the detection wavelength of emission, and δ the average angle between absorption and emission dipoles ($r_0 = 0.2(3 \cos^2 \delta - 1)$). [b] The excitation wavelength, 403 nm, was applied to all samples. The χ^2 values of the fittings were maintained as $\sim$1.0$-$1.4. The standard deviations were obtained by exponential fitting procedures using a program "Origin 6.0".
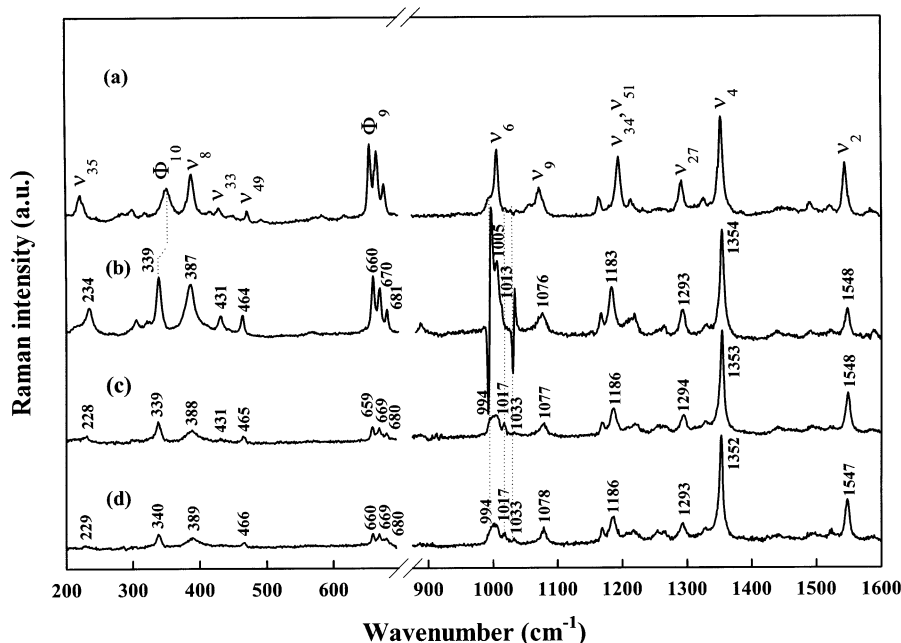

Figure 7. Resonance Raman spectra by 458 nm excitations of (a) Z2 in THF, (b) PyZ2 in pyridine, (c) PyZ2 in THF, and (d) PyZ2 in CH$_2$Cl$_2$. The Raman band assignments of Z2 are given in panel a.

pyridine solvent coordination. Especially, the intermolecular coordination in the porphyrin box induces five-coordination of the central Zn^{2+} metal of PyZ2, as well as doming of the porphyrin ring, which leads to mean plane deviation by pulling the central Zn^{2+} ion out of the plane by $\sim$0.05 Å.[12] As a similar system, the coordination of zinc(II) porphyrin by imidazole produces 5-cm^{-1} downshifts in the ν_4 and ν_2 bands, which are induced by the five-coordinated and domed zinc(II) porphyrin structure.[28] Finally, we can observe new Raman bands in Figure 7b$-$d and Table 4, which originate from the coordinated pyridine solvent or the coordinated pyridyl group. Although the Raman bands at 994 and 1033 cm^{-1} are due to free pyridine solvent, the bands at 1013 cm^{-1} in Figure 7b and at 1017 cm^{-1} in Figure 7c and d are contributed by the coordinated pyridine solvent and the coordinated pyridyl group. According to the previous Raman study on various pyridine$-$metal complexes, the ν_1 mode of pyridine (at $\sim$1000 cm^{-1}) is known to be very sensitive to the force constant of N$-$M stretching between coordinated pyridine and metal.[29] This mode was reported to

exhibit a frequency upshift as the force constant of N$-$M stretching was increased,[29] similar to that observed in Figure 7b and c.

Dipole$-$Dipole Interaction and Energy-Transfer Process in Porphyrin Box. To explain the blue shift of the low-energy Soret band in the porphyrin box (see Figure 1e,f), the following intramolecular and intermolecular excitonic dipole coupling scheme is introduced. The intramolecular and intermolecular couplings imply coupling within the zinc(II) porphyrin dimer and between zinc(II) porphyrin dimers, respectively. The Soret band splitting in the porphyrin dimer, which is presented in Figure 1a$-$d, can be explained by intramolecular excitonic dipole couplings within the orthogonally linked porphyrin dimers.[5,24] As shown in Scheme 2, two degenerate transition dipole moments (B_x and B_y) create one Soret band in the porphyrin monomer. However, dipole couplings (B_z-B_z at opposite, B_x-B_y at orthogonal, B_z-B_z at parallel) between the porphyrin monomer units generate three nondegenerate transi-

TABLE 4: Normal Modes of PyZ2 in Pyridine, THF, and CH$_2$Cl$_2$

	local coordinate	symmetry	Assignment[a]		
			pyridine	THF	CH$_2$Cl$_2$
ν_{35}	ν(pyr-transl)	B_{2g}	234	228	229
ϕ_{10}	ν(por-ph)	A_{1g}	339	339	340
ν_8	ν(NM)	A_{1g}	387	388	389
ν_{33}	ν(pyr-rot)	B_{2g}	431	431	
ν_{49}	ν(pyr-rot)	E_u	464	465	466
ϕ_9	$\delta(C_\alpha C_m C_\alpha) + \nu_{6a}(Ph)$	A_{1g}(antisym)	660	659	660
ϕ_9	$\delta(C_\alpha C_m C_\alpha) + \nu_{6a}(Ph)$	E_u(both)	670	669	669
$\phi_{9''}$	$\delta(C_\alpha C_m C_\alpha) + \nu_{6a}(Ph)$	A_{1g}(sym)	681	680	680
ν(pyridine)	free	A_{1g}	994	994	994
ν_6	ν(pyr-breath)	A_{1g}	1005	1005	1005
ν(pyridine)	coordinated	A_{1g}	1013	1017	1017
ν(pyridine)	free	A_{1g}	1033	1033	1033
ν_9	$\delta(C_\beta H)_{sym}$	A_{1g}	1076	1077	1078
ν_{34}	$\delta(C_\beta H)_{asym}$	B_{2g}	1183	1186	1186
ν_{51}	$\delta(C_\beta H)_{asym}$	E_u	1183	1186	1186
ν_{27}	$\nu(NC_\alpha) + \nu(C_m C_{ph})$	B_{2g}	1293	1294	1293
ν_4	ν(pyr half-ring)$_{sym}$	A_{1g}	1354	1353	1352
ν_2	$\nu(C_\beta C_\beta)$	A_{1g}	1548	1548	1547

[a] The assignments were based on the previous normal-mode analyses of sample Z2 in THF.[24]

SCHEME 2
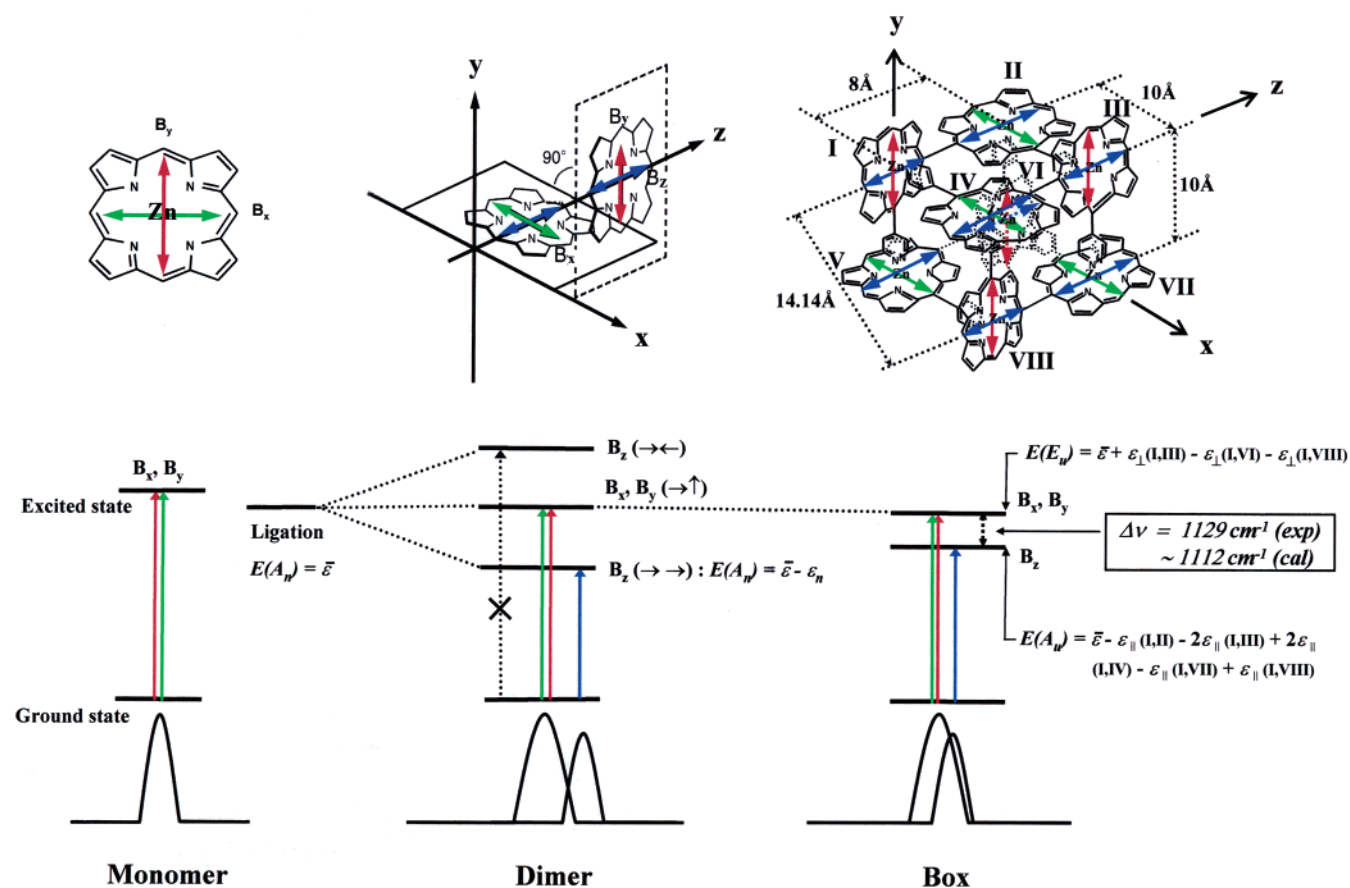
tion dipoles and concomitantly two separated Soret bands in the orthogonally linked porphyrin dimer. In Scheme 2, the B_z–B_z opposite dipole coupling is a forbidden transition, because of its zero-transition dipole moment, whereas the B_x–B_y orthogonal and B_z–B_z parallel dipole couplings generate the same and lower-energy Soret bands, with respect to the Soret band of the porphyrin monomer.

On the other hand, some complicated intramolecular and intermolecular dipole interactions must be considered in the Soret band splitting of the porphyrin box (see Scheme 2), because the porphyrin box has a rigorously rigid and close-

proximity intermolecular coordination geometry (10 Å × 10 Å × 8 Å).[12] As a similar molecular system, an orthogonally self-assembled cyclic porphyrin tetramer exhibited Soret band splitting, because of its excitonic dipole–dipole coupling between the porphyrin monomer units (mono-(4-pyridyl)-triphenylporphyrin).[20] Thus, the formation of the three-dimensional box is expected to induce the splitting of the Soret band, which would invoke dipole–dipole excitonic interactions in the S$_2$ state between eight mutually perpendicular porphyrin molecules. The octamer geometry is assumed to have C_{4h} symmetry, similar to the tetramer.

The ground-state wave function of the octamer (ψ_g) is

$$\psi_g = \psi_I \psi_{II} \psi_{III} \psi_{IV} \psi_V \psi_{VI} \psi_{VII} \psi_{VIII} \tag{1}$$

where ψ_I, ψ_{II}, ψ_{III}, ψ_{IV}, ψ_V, ψ_{VI}, ψ_{VII}, and ψ_{VIII} represent the ground-state wave functions of porphyrin molecules respectively numbered I, II, III, IV, V, VI, VII, and VIII as shown in Scheme 2. The wave function for molecule I to be excited with a transition dipole moment M_u either parallel ($u = \parallel$) or perpendicular ($u = \perp$) to the fourfold axis (the z-axis in Scheme 2) can then be written as

$$\psi_{I,u} = \psi^*_{I,u} \psi_{II} \psi_{III} \psi_{IV} \psi_V \psi_{VI} \psi_{VII} \psi_{VIII} \ (u = \parallel, \perp) \tag{2}$$

and similarly for excitations that are localized on molecules II, III, IV, V, VI, VII, and VIII.

The excitonic wave functions that result from coupling V between these localized states have the general form

$$|k, u\rangle = \frac{1}{2\sqrt{2}} \sum_{j=1}^{VIII} \exp\left(\frac{2\pi kji}{4}\right) \psi_{j,u} \tag{3}$$

The sixteen possible states—with $k = 0, \pm1, \pm2, \pm3, 4$ and $u = \parallel$ or $\perp$—span the irreducible representations of the C_{4h} group. Of these possible states, only state $|0, \parallel\rangle$ (A_u) and the twofold degenerate state $|\pm1, \perp\rangle$ (E_u) are connected by dipole-allowed transitions to the A_g ground state, Ψ_g.

The wave functions of these states are given as

$$|0, z\rangle = \frac{1}{2\sqrt{2}}(\Psi_{I,\parallel} - \Psi_{II,\parallel} - \Psi_{III,\parallel} + \Psi_{IV,\parallel} + \Psi_{V,\parallel} - \Psi_{VI,\parallel} -$$
$$\Psi_{VII,\parallel} + \Psi_{VIII,\parallel}) \ (A_u) \tag{4}$$

$$|1, x\rangle = \frac{1}{2}(\Psi_{II,\perp} + \Psi_{V,\perp} - \Psi_{IV,\perp} - \Psi_{VII,\perp})$$

$$|1, y\rangle = \frac{1}{2}(\Psi_{I,\perp} + \Psi_{III,\perp} - \Psi_{VI,\perp} - \Psi_{VIII,\perp})(E_u)$$

From eqs 2 and 4, it follows by inspection of Scheme 2 that the energies of the allowed transitions are

$$E(A_u) = \bar{\epsilon} - \epsilon_\parallel(I,II) - 2\epsilon_\parallel(I,III) + 2\epsilon_\parallel(I,IV) - \epsilon_\parallel(I,VII) +$$
$$\epsilon_\parallel(I,VIII)$$

$$E(E_u) = \bar{\epsilon} + \epsilon_\perp(I,III) - \epsilon_\perp(I,IV) - \epsilon_\perp(I,VIII) \tag{5}$$

where $\bar{\epsilon}$ is the energy of the locally excited state plus the energy change of the constituents in the octamer due to excitation, and ϵ is the coupling energy between the transition dipoles, e.g., $\epsilon_\parallel(I,II) = \langle\Psi_{I,\parallel}|V|\Psi_{II,\parallel}\rangle$ and $\epsilon_\perp(I,III) = \langle\Psi_{I,\perp}|V|\Psi_{III,\perp}\rangle$, where V is the intermolecular perturbation potential,[30−32] e.g.,

$$V_{AB} = \frac{|\mu_A \mu_B|}{4\pi\epsilon_0 R^3}(2\cos\theta_A \cos\theta_B + \sin\theta_A \sin\theta_B \cos\varphi) \tag{6}$$
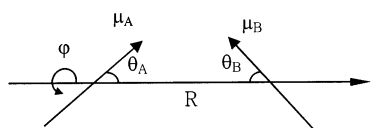
The angles noted in eq 6 define the relative orientations of the transition moments in molecules A and B.[32]

Now, we can calculate the energy splitting (ΔE) between the two allowed transitions, using the reported dipole strength

$(9.5 \pm 0.5 \text{ D})$[20] of the Soret band of the pyridyl-substituted zinc(II) porphyrin monomer and the porphyrin center-to-center distances within PyZ2 and between PyZ2 molecules in the porphyrin box (8 and 10 Å, respectively).[12] Using the point−dipole approximation[30−32] for V, the coupling energies are calculated to be $\epsilon_\parallel(I,II) = 1773.5 \text{ cm}^{-1}$, $\epsilon_\parallel(I,III) = 179.7 \text{ cm}^{-1}$, $\epsilon_\parallel(I,IV) = 454.0 \text{ cm}^{-1}$, $\epsilon_\parallel(I,VII) = 91.5 \text{ cm}^{-1}$, $\epsilon_\parallel(I,VIII) = 160.6 \text{ cm}^{-1}$, $\epsilon_\perp(I,III) = 216.5 \text{ cm}^{-1}$, $\epsilon_\perp(I,VI) = 179.7 \text{ cm}^{-1}$, and $\epsilon_\perp(I,VIII) = 80.3 \text{ cm}^{-1}$. The energy splitting ΔE between the two allowed transitions of the octamer is calculated to be $\sim$1112 cm^{-1}, in good agreement with the experimental splitting value of 1129 cm^{-1}, which is the energy difference between the high- and low-energy Soret bands of the porphyrin box (see data for PyZ2 in CH$_2$Cl$_2$ in Table 1). The exciton model in Scheme 2 also indicates that the high-energy Soret band reveals a red shift of $\sim$43.5 cm^{-1} in the porphyrin box, with respect to the ligated dimer position, resulting from excitonic dipole−dipole interactions between four parallel transition dipole moments along the **x**- or **y**-axis. The experimental value that corresponds to this interaction is 78 cm^{-1}, which is the energy difference between the high-energy Soret bands of the dimer and the porphyrin box (see data for PyZ2 in pyridine and PyZ2 in CH$_2$Cl$_2$ in Table 1). However, this value is too small to be resolved in the absorption spectrum or from the ligation and rigidity effects on the absorption spectra. Although the enhanced ligation strength induces the red shift in the absorption spectrum, the increased rigidity[33] results in the blue shift. Nevertheless, these effects cannot explain the irregular absorption band shifts in the porphyrin box, e.g., the red shift in the high-energy Soret band and the blue shift in the low-energy Soret band. The irregular band shifts in the porphyrin box are due to excitonic interactions between four parallel transition dipole moments along the **x**- or **y**-axis, as well as excitonic interactions between eight parallel transition dipole moments along the **z**-axis (see Scheme 2). This process is regarded as a dipole redistribution process within the three-dimensional zinc(II) porphyrin box.

The excitonic dipole−dipole resonance interaction between the porphyrin units is expected to stimulate an energy-transfer process in the three-dimensional zinc(II) porphyrin box. The self-assembled cyclic zinc(II) porphyrin tetramer also showed a fast anisotropy decay time of $\sim$31 ps, which was ascribed to the Förster-type singlet energy-transfer process between the neighboring porphyrin monomer units.[22,34] To examine the excitation energy-transfer process of the porphyrin box, femtosecond transient absorption anisotropy decay measurements were performed for the porphyrin box (see Figure 8 a). Transient absorption anisotropy decay of PyZ2 was also measured, as a reference (Figure 8b). As shown in Figure 8b, PyZ2 reveals slow transient absorption decay and concomitantly does not show any anisotropy decay profile in a time region of tens of picoseconds, which is similar to the previous Z2 and orthogonally linked porphyrin arrays.[6] The very fast anisotropy decay of $\sim$200 fs that results from the B_x and B_y equilibrium process inside the porphyrin monomer and the coherent excitation energy transfer to the adjacent intra unit in Z2 was not observed within this relatively slow time scale.

On the other hand, the porphyrin box shows a relatively fast transient absorption anisotropy rise of 12 ± 3 ps (Figure 8a). This fast anisotropy rise time is indicative of the excitation energy-transfer process of the porphyrin box that results from the excitonic dipole−dipole resonance interactions within the porphyrin box. It is noteworthy that the porphyrin box has a shorter energy-transfer time (12 ± 3 ps) than that of the cyclic porphyrin tetramer ($\sim$31 ps), even though they have the same

Photophysical Properties of 3D Zinc(II) Porphyrin

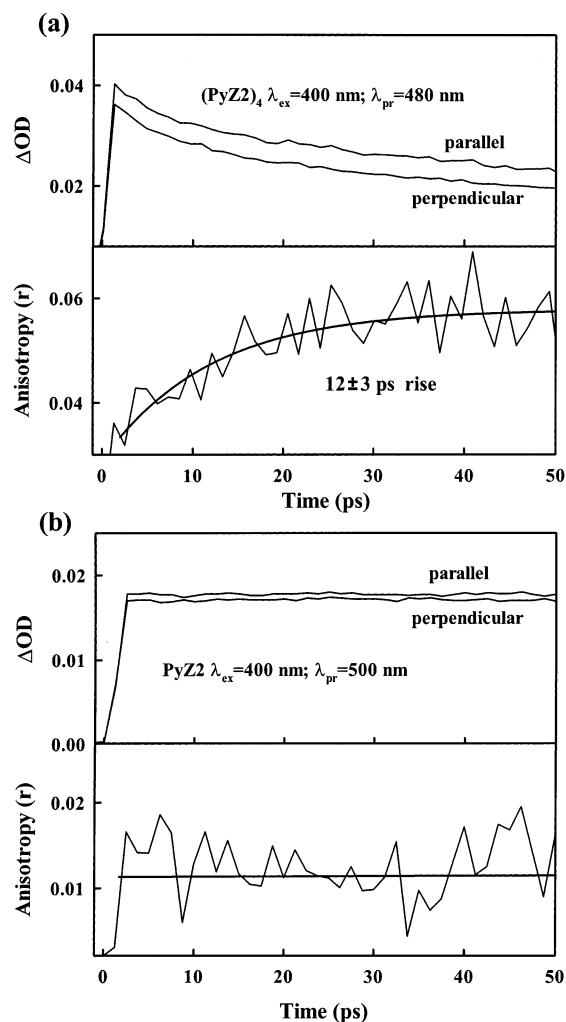*J. Phys. Chem. B, Vol. 107, No. 37, 2003* **9987**

Figure 8. Transient absorption decay profiles of PyZ2 in (a) CH₂Cl₂ and (b) pyridine for parallel and perpendicular orientations of pump and probe polarizations and their anisotropy decays.

center-to-center distance (10 Å) between nearest intermolecular porphyrin units. This result implies that the rigid intermolecular coordination geometry of the porphyrin box accelerates the excitation energy-transfer rate between the porphyrin units.

Conclusions

There have been numerous efforts on the synthesis of covalently linked porphyrin arrays using a variety of linkers, which inevitably requires elaborate and time-consuming work. As a supplementary route in the preparation of porphyrin arrays, a synthetic strategy that uses a supramolecular chemistry has been envisaged, because it provides versatility in molecular networking in three-dimensional space, to increase the efficiency in light harvesting and electronic communication. As the molecular structures become complicated in space, it is also indispensable to understand interchromophoric interactions, such as exciton coupling and an energy migration process. In this regard, we have investigated various photophysical properties of the porphyrin box that have been prepared by intermolecular coordination of the orthogonally linked porphyrin dimer (PyZ2). The porphyrin box, i.e., $(PyZ2)_4$, causes red shifts in the high-energy Soret and Q absorption bands, as well as blue shifts in the low-energy Soret and fluorescence bands, with respect to its constituent unit (Z2 and PyZ2). Although the red-shifted high-energy Soret and Q bands are characteristic of ligated

metalloporphyrins, the blue shifts in the low-energy Soret band and fluorescence spectra are unique features of the three-dimensional self-assembled zinc(II) porphyrin box. The blue-shifted low-energy Soret band is the result of excitonic dipole–dipole interactions between eight parallel transition dipole moments of the porphyrin units along the *z*-axis of the porphyrin box. In addition, the blue-shifted fluorescence is due to the minimized electronic interaction between the porphyrin monomer units, which originates from the enhanced rigidity in the $(PyZ2)_4$ assembly. The porphyrin box exhibits the enhancement of the short-lived (~1 ns) fluorescence decay component, as well as the shifts of the ν_2 and ν_4 Raman bands, being indicative of perturbed porphyrin planarity in the porphyrin box. The macromolecular porphyrin box also reveals a relatively slow rotational diffusion time of ~4.7 ns. The fast anisotropy rise time of 12 ± 3 ps in the femtosecond transient absorption anisotropy decay measurement reflects an efficient excitation energy-transfer process within the rigid three-dimensional zinc(II) porphyrin box, which results from the excitonic dipole–dipole resonance interactions between the porphyrin units. Overall, our investigations on various photophysical properties of the three-dimensional porphyrin box afford the opportunity to elucidate the relationship between molecular structures in three-dimensional molecular networks and exciton coupling/transport processes.

References and Notes

(1) Lin, V. S.; Dimagno, S. G.; Therien, M. J. *Science* **1994**, *264*, 1105.

(2) Kodis, G.; Liddell, P. A.; de la Garza, L.; Clausen, P. C.; Lindsey, J. S.; Moore, A. L.; Moore, T. A.; Gust, D. *J. Phys. Chem. A* **2002**, *106*, 2036.

(3) Hilmey, D. G.; Abe, M.; Nelen, M. I.; Stilts, C. E.; Baker, G. A.; Baker, S. N.; Bright, F. V.; Davies, S. R.; Gollnick, S. O.; Oseroff, A. R.; Gibson, S. L.; Hilf, R.; Detty, M. R. *J. Med. Chem.* **2002**, *45*, 449.

(4) Yang, S. I.; Seth, J.; Balasubramanian, T.; Kim, D.; Lindsey, J. S.; Holten, D.; Bocian, D. F. *J. Am. Chem. Soc.* **1999**, *121*, 4008.

(5) Kim, Y. H.; Jeong, D. H.; Kim, D.; Jeoung, S. C.; Cho, H. S.; Kim, S. K.; Aratani, N.; Osuka, A. *J. Am. Chem. Soc.* **2001**, *123*, 76.

(6) Cho, H. S.; Song, N. W.; Kim, Y. H.; Jeoung, S. C.; Hahn, S.; Kim, D.; Kim, S. K.; Yoshida, N.; Osuka, A. *J. Phys. Chem. A* **2000**, *104*, 3287.

(7) Cho, H. S.; Jeong, D. H.; Cho, S.; Kim, D.; Matsuzaki, Y.; Tanaka, K.; Tsuda, A.; Osuka, A. *J. Am. Chem. Soc.* **2002**, *124*, 14642.

(8) Ogawa, K.; Zhang, T.; Yoshihara, K.; Kobuke, Y. *J. Am. Chem. Soc.* **2002**, *124*, 22.

(9) Chernook, A. V.; Rempel, U.; van Borczyskowski, C.; Shulga, A. M.; Zenkevich, E. I. *Chem. Phys. Lett.* **1996**, *254*, 229.

(10) Guldi, D. M.; Ros, T. D.; Braiuca, P.; Prato, M.; Alessio, E. *J. Mater. Chem.* **2002**, *12*, 2001.

(11) Alessio, E.; Geremia, S.; Mestroni, S.; Iengo, E.; Srnova, I.; Slouf, M. *Inorg. Chem.* **1999**, *38*, 869.

(12) Tsuda, A.; Nakamura, T.; Sakamoto, S.; Yamaguchi, K.; Osuka, A. *Angew. Chem., Int. Ed.* **2002**, *41*, 2817.

(13) Bailey, M. F.; Thompson, E. H. Z.; Millar, D. P. *Methods* **2001**, *25*, 62.

(14) Kyoung, M.; Kim, S. Y.; Seok, H.-Y.; Park, I.-S.; Lee, M. *Biochim. Biophys. Acta* **2002**, *1598*, 74.

(15) Osuka, A.; Shimidzu, H. *Angew. Chem., Int. Ed. Engl.* **1997**, *36*, 135.

(16) Lewis, C.; Ware, W. R.; Doemeny, L. J.; Nemzek, T. L. *Rev. Sci. Instrum.* **1973**, *44*, 107.

(17) Wild, U. P.; Holzwarth, A. R.; Good, H. P. *Rev. Sci. Instrum.* **1977**, *48*, 1621.

(18) Kim, Y.-R.; Hahn, J.-S.; Hong, H.; Jeong, W.; Song, N. W.; Shin, H.-C.; Kim, D. *Biochim. Biophys. Acta* **1999**, *1429*, 486.

(19) Mizutani, T.; Wada, K.; Kitagawa, S. *J. Org. Chem.* **2000**, *65*, 6097.

(20) Yatskou, M. M.; Koehorst, R. B. M.; Donker, H.; Schaafsma, T. J. *J. Phys. Chem. A* **2001**, *105*, 11425.

(21) Bellacchio, E.; Sauer, K. *J. Phys. Chem. B* **1999**, *103*, 2279.

(22) Yatskou, M. M.; Koehorst, R. B. M.; van Hoek, A.; Donker, H.; Schaafsma, T. J.; Gobets, B.; van Stokkum, I.; van Grondelle, R. *J. Phys. Chem. A* **2001**, *105*, 11432.

(23) Sazanovich, I. V.; Galievsky, V. A.; van Hoek, A.; Schaafsma, T. J.; Malinovskii, V. L.; Holten, D.; Chirvony, V. S. *J. Phys. Chem. B* **2001**, *105*, 7818.

(24) Jeong, D. H.; Yoon, M.-C.; Jang, S. M.; Kim, D.; Cho, D. W.; Yoshida, N.; Aratani, N.; Osuka, A. *J. Phys. Chem. A* **2002**, *106*, 2359.

(25) Li, X.-Y.; Czernuszewicz, R. S.; Kincaid, J. R.; Su, Y. O.; Spiro, T. G. *J. Phys. Chem.* **1990**, *94*, 31.

(26) Li, X.-Y.; Czernuszewicz, R. S.; Kincaid, J. R.; Spiro, T. G. *J. Am. Chem. Soc.* **1989**, *111*, 7012.

(27) Jentzen, W.; Simpson, M. C.; Hobbs, J. D.; Song, X.; Ema, T.; Nelson, N. Y.; Medforth, C. J.; Smith, K. M.; Veyrat, M.; Mazzanti, M.; Ramasseul, R.; Marchon, J.-C.; Takeuchi, T.; Goddard, W. A.; Shelnutt, J. A. *J. Am. Chem. Soc.* **1995**, *117*, 11085.

(28) Feitelson, J.; Spiro, T. G. *Inorg. Chem.* **1986**, *25*, 861.

(29) Wu, D.-Y.; Ren, B.; Jiang, Y.-X.; Xu, X.; Tian, Z.-Q. *J. Phys. Chem. A* **2002**, *106*, 9042.

(30) Kasha, M. *Radiat. Res.* **1963**, *20*, 55.

(31) Kasha, M.; Rawls, H. R.; El-Bayoumi, M. A. *Pure Appl. Chem.* **1965**, *11*, 371.

(32) Scholes, G. D.; Ghiggino, K. P. *J. Phys. Chem.* **1994**, *98*, 4580.

(33) Kim, D.; Osuka, A. *J. Phys. Chem. A*, in press. (Review article.)

(34) Yatskou, M. M.; Donker, H.; Novikov, E. G.; Koehorst, R. B. M.; van Hoek, A.; Apanasovich, V. V.; Schaafsma, T. J. *J. Phys. Chem. A* **2001**, *105*, 9498.